Anisotropic flux pinning in a network of planar defects

A. Gurevich and L. D. Cooley*
Applied Superconductivity Center, University of Wisconsin, Madison, Wisconsin 53706
(Received 26 May 1994)

We consider a strong flux pinning by a network of high-j_c planar defects which can result in high macroscopic critical current densities J_c in bulk superconductors. Such a pinning potential gives rise to a qualitative change of the structure of normal cores which turn into highly anisotropic phase cores described by equations of nonlocal Josephson electrodynamics. We obtained a solution of these equations for a vortex parallel to the planar defect and calculated the magnetic-field distribution and the transversal pinning force $f_\perp$ between the vortex and the defect. The longitudinal pinning force $f_\parallel$ of vortices along the defect is determined by both their magnetic interaction with pinned intragrain fluxons and local inhomogeneities of the defect. The force $\mathbf{f}(H)$ is shown to be highly anisotropic with respect to the current direction, the value $f_\parallel$ along the defect being much smaller than the perpendicular component $f_\perp$. This can result in the preferential flux motion along the percolative paths formed by planar defects, giving rise to a nonmonotonic $J_c(H)$ dependence due to the increase of $f_\parallel$ with H caused by magnetic interaction of inter- and intragrain fluxons. The effect of topology of the pinning network on J_c and flux creep is discussed. We also calculate the low-field dependences of $J_c(H)$ and consider the regions of the T-H space, where a magnetic granularity transition can occur.

I. INTRODUCTION

Pinning in superconductors with high critical current densities J_c is often due to a dense network of planar crystalline defects. For low-T_c superconductors (LTS's) the characteristic examples are the optimized Nb-Ti, where the extremely strong pinning is caused by a network of thin α-Ti ribbons,[1] or the grain-boundary pinning in Nb_3Sn,[2] Chevrel phases,[3,4] and NbN.[5] A similar situation may take place in high-T_c superconductors (HTS's) which also contain numerous planar defects, such as twins in $YBa_2Cu_3O_{7-x}$,[6-8] stacking faults,[9,10] colonies of low-angle c-axis grain boundaries,[9-12] or "brick-wall" structures of twist grain boundaries[13] in Bi-based superconductors.

In such high-J_c materials, pinning is due to coherent defect structures which usually do not cause strong distortions of crystalline lattice and thereby do not result in a significant degradation of superconducting properties. This fact reflects two essential features of high-J_c superconductors. On the one hand, the most effective pinning can be proved by a dense network of planar defects parallel to the flux lines. However, unlike the case of randomly distributed point pins, the network of planar defects can block or divert the macroscopic current flow if the tunneling superconducting current density j_c through the pins is smaller than J_c determined by flux pinning. At $J_c > j_c$, the pinning structure can give rise to the magnetic granularity which manifests itself in a drop of the transport J_c due to the appearance of closed current loops within macroscopic crystalline grains, where densities of circulating magnetization currents become larger than J_c.[14,15] These opposite tendencies seem to be reconciled in the optimized Nb-Ti, where the strong pinning is due to a dense network of thin α-Ti ribbons with thicknesses smaller or of the order of the coherence length ξ.[1] This fact provides the strong proximity coupling of the pinning structure with the Nb-Ti matrix, which, in turn, can result in a very high j_c of the order of the depairing current density j_d.

Such a network of high-j_c planar defects does not give rise to weakly pinned Josephson (J) vortices[16] whose dissipative motion along the defects eventually results in the superconducting decoupling of crystalline grains. Therefore these high-j_c planar pins do not cause the magnetic granularity, but rather play the role of "hidden" weak links strongly deforming the normal cores of Abrikosov (A) vortices which turn into Abrikosov vortices with highly anisotropic Josephson cores[17,18] (hereafter such vortices are called AJ vortices). For a single planar defect, the Josephson core is a 2π phase kink

$$\varphi(x)=\pi+2\tan^{-1}\left[\frac{x}{l}\right], \tag{1}$$

$$l=\frac{\lambda_J^2}{\lambda}=\frac{3\sqrt{3}}{4}\frac{j_d}{j_c}\xi, \tag{2}$$

of length l along the defect and of width ξ in the transversal direction.[17] Here $\varphi(x)$ is the phase difference across the contact, $\lambda_J=(c\phi_0/16\pi^2\lambda j_c)^{1/2}$ is the Josephson magnetic penetration depth, λ is the London penetration depth, ϕ_0 is the flux quantum, c is the speed of light, and $j_d=c\phi_0/12\sqrt{3}\pi^2\lambda^2\xi$. The AJ phase core is surrounded by circulating screening currents which decay over the

0163-1829/94/50(18)/13563(14)/$06.00

London penetration depth λ. Such a vortex arises if the core size l is smaller than λ, which occurs in the case of strong Josephson coupling when $\lambda_J(j_c)$ becomes smaller than λ, that is, $j_l < j_c < j_d$, where

$$j_l = \frac{c\phi_0}{16\pi^2\lambda^3} \simeq \frac{j_d}{\kappa} \tag{3}$$

for bulk superconductors and $j_l \sim j_d \xi d/\lambda^2$ for thin films of thickness $d \ll \lambda$,[17,19] where $\kappa = \lambda/\xi$ is the Ginzburg-Landau parameter (hereafter we consider the case of extreme type-II superconductors for which $\kappa = \lambda/\xi \gg l$). The condition $j_c > j_l$ can fulfill in high-J_c materials, in particular, the value $j_l = 8\times10^5$ A/cm^2 for Nb-Ti at 4.2 K ($\lambda \approx 250$ nm) is smaller than $J_c \approx 2\times10^6$ A/cm^2 observed on the optimized Nb-Ti at $H = 0$.[1] In this case the concentration of α-Ti ribbons is so high that the transport current may flow through the pins, therefore j_c is larger than J_c, and $j_c > j_l$. Notice that the disappearance of normal cores in AJ vortices can be caused by any crystalline defect with $j_c < j_d$.

The geometry of the planar defect network is also important. For instance, in twin domains with different orientations with respect to the crystallographic axes,[6-8] the planar defects can divert the local current flow, limiting the macroscopic J_c due to reduction of the current-carrying cross-sectional area. In a random network of planar defects with the density of pins exceeding the percolation threshold, the supercurrent must cross several defects, which would offset the increase of J_c due to flux pinning. Such a random network is known to have a complicated topological structure in which only a small part of the defects belong to the percolative path.[20] In general, both regimes in which the planar defects act as pinning centers, or block (divert) the current flow coexist, their relative contributions depending on both j_c and the geometry of the pinning network. In this paper we consider flux pinning by a network of planar high-j_c crystalline defects which are modeled by high-j_c Josephson contacts. In such an approach the pinning potential $U(\mathbf{r})$ is mostly determined by the geometry of pinning network, whereas the specific mechanisms of the Josephson tunneling manifest themselves only via the amplitude of j_c and its temperature and field dependences [as a characteristic example of high-j_c weak links we consider here strongly proximity coupled normal (N) layer in a superconducting (S) matrix].

Therefore, in order to calculate $\mathbf{f}$, one has to consider the interaction of the A vortex with planar Josephson contacts. This interaction cannot be described within the framework of conventional local Josephson electrodynamics employed for the description of J vortices in long Josephson contacts, since it assumes that $\varphi(y)$ varies along the contact over lengths much larger than λ. By contrast, the main contribution to the pinning forces comes from intragrain A vortices spaced from the grain boundaries by distances $s \ll \lambda$. In this case $\varphi(y)$ changes over lengths $\sim s$ much shorter than λ, so $\varphi(y)$ is described by equations of a nonlocal Josephson electrodynamics (NJE) in which $\varphi(y)$ can vary over much smaller spatial scale than that of $H(y)$.[17,21] NJE equations enable one to take account of variations of $\varphi(y)$ over any lengths larger than ξ provided that the planar defect can still be regarded as a weak link ($j_c \ll j_d$) for which the tunneling currents are too small to affect the superconducting gap Δ outside the contact. In this case the interaction of vortices with high-j_c planar defects can result in the transformation of normal cores of A vortices into the phase AJ cores described by NJE equations which account for the change of the core structure by the pinning potential. This approach differs from the previous calculations of the vortex interaction with twins[22,23] performed within the framework of the Ginzburg-Landau equations (the case of the vortex perpendicular to the contact was considered in Refs. 13 and 24). The paper is organized as follows.

In Sec. II, NJE equations which describe the interaction of the A vortex with parallel planar Josephson contact are derived. We obtained an analytical solution of these equations, $\varphi(y,x)$, in the nonlocal regime $j_c > j_1$ and traced the change of the field distribution in the A vortex as it moves toward the planar defect, including the disappearance of the normal core and appearance of the AJ phase core at $s \sim \xi$.

In Sec. III, the attraction force $f_\perp(s)$ between the A vortex and the parallel Josephson contact is calculated. It is shown that, depending on the vortex distance s from the contact, there are two characteristic regimes: at $s < l$ the force $f_\perp(s) \propto 1/s$ has the magnetic origin, similar to a vortex parallel to the sample surface. At $l \ll s \ll \lambda$, the planar defect becomes transparent for the vortex screening currents, and the force $f_\perp(s)$ decreases as $1/s^2$.

In Sec. IV we consider the longitudinal elementary pinning force $f_\parallel$ which is due to both inhomogeneities of $j_c(\mathbf{r})$ along the defect and the magnetic interaction of intergrain AJ vortices with intragrain A fluxons. It is shown that $f_\parallel \ll f_\perp$ because of the strong anisotropy of the phase AJ core, the interaction with intragrain A fluxons giving rise to the increase of $f_\parallel(H) \propto H^{1/2}$ with H. As a result, the planar defects can become channels for the preferential motion of vortices.

In Sec. V, the elementary pinning force $\mathbf{f}$ calculated in the previous sections is used to evaluate the low-field dependence of $J_c(H)$ in a network of planar defects. It is shown that J_c strongly depends on the topology of the pinning network and can be determined by either the longitudinal component $f_\parallel$ along flux percolative paths formed by the grain boundaries, or the perpendicular component $f_\perp$ averaged over the grain surface. The crossover between different pinning regimes can give rise to a nonmonotonic field dependence of $J_c(H)$ (the so-called, "fishtail effect"). In both cases $J_c(H)$ depends weakly on the microscopic properties of planar pins, and is mostly determined by the geometry of the pinning network, in particular, J_c turns out to be inversely proportional to a characteristic grain size, D, at $D \gg l$. It is shown that the magnetic granularity may arise at large H due to the overlapping of the AJ phase cores.

In Sec. VI we discuss implications of the obtained results to some high-J_c materials.

II. TRANSVERSAL PINNING FORCE

A. NJE equations

In this section we derive stationary NJE equations for the phase distribution $\varphi(y,s)$, induced by the A vortex on the planar defect being at a distance s from the vortex (Fig. 1). The z component $H(x,y)$ of the magnetic field $\mathbf{H}$ obeys the London equation

$$H-\lambda^2\left[\frac{\partial^2 H}{\partial x^2}+\frac{\partial^2 H}{\partial y^2}\right]=\phi_0\delta(x-s)\delta(y)+\frac{\phi_0\varphi'(y)}{2\pi}\delta(x)\ , \tag{4}$$

where the prime denotes the derivative over y, and the defect thickness is assumed to be negligible. The last term in Eq. (4) ensures the well-known boundary condition on the Josephson contact,[16]

$$\varphi'(y)=\frac{8\pi^2\lambda^2}{c\phi_0}[j_y(x=+0,y)-j_y(x=-0,y)]\ , \tag{5}$$

where j_y is the component of the current density $\mathbf{j}$ parallel to the defect. Indeed, integrating Eq. (4) from $x=-0$ to $x=+0$ and using the continuity of $H(x,y)$ at $x=0$, we obtain

$$\lambda^2\left[\frac{\partial H(x=+0)}{\partial x}-\frac{\partial H(x=-0)}{\partial x}\right]=-\phi_0\frac{\varphi'}{2\pi}\ , \tag{6}$$

Eq. (6) reduces to Eq. (5) after using the Maxwell equation $\partial H/\partial x=-4\pi j_y/c$.

Making use of the Green's function of the London equation, Eq. (4) can be solved as follows:

$$H(x,y)=\frac{\phi_0}{2\pi\lambda^2}K_0\left[\frac{\sqrt{(x-s)^2+y^2}}{\lambda}\right]+\frac{\phi_0}{4\pi^2\lambda^2}\int_{-\infty}^{\infty}\varphi'(u)K_0\left[\frac{\sqrt{x^2+(y-u)^2}}{\lambda}\right]du\ , \tag{7}$$

where $K_0(x)$ is a modified Bessel function, the first term in the right-hand side is the field of A vortex,[25] and the second term describes the influence of the defect. By integrating Eq. (7) over x and y (see, e.g., Ref. 26), we can calculate the total magnetic flux ϕ in the form

$$\phi=\phi_0+[\varphi(\infty)-\varphi(-\infty)]\frac{\phi_0}{2\pi}\ . \tag{8}$$

Therefore, ϕ equals ϕ_0 for any $\varphi(y)$ with $\varphi(\infty)=\varphi(-\infty)=0$. If $\varphi(y)$ is a $2\pi n$ phase kink for which $\varphi(\infty)-\varphi(-\infty)=\pm 2\pi n$, the flux ϕ is quantized: $\phi=(1\pm n)\phi_0$, where $n=1,2,\ldots$.

In order to obtain a self-consistent equation for $\varphi(y)$, we use the continuity of the normal component $j_x(x,y)$ flowing through the planar defect,

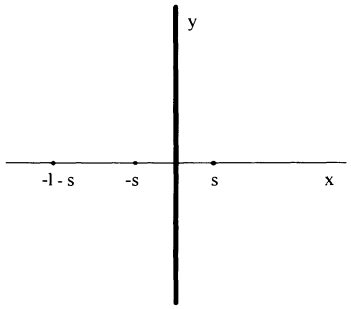

FIG. 1. Abrikosov (A) vortex at $x=s$ parallel to the planar defect being in the yz plane. The points at $x=-s$ and $x=-s-l$ show the positions of "image" antivortex and vortex, respectively, (see the text).

$$\frac{c}{4\pi}\frac{\partial H}{\partial y}=j_c\sin\varphi\ . \tag{9}$$

Substituting Eq. (7) into Eq. (9), we arrive at the following equation for $\varphi(y)$:

$$\int_{-\infty}^{\infty}\varphi'(u)K_1\left[\frac{|y-u|}{\lambda}\right]\mathrm{sgn}(y-u)\frac{du}{\pi}+\frac{2y}{\sqrt{s^2+y^2}}K_1\left[\frac{\sqrt{s^2+y^2}}{\lambda}\right]+\frac{\lambda}{l}\sin\varphi=0\ . \tag{10}$$

Now we calculate the free energy, $F=F_J+F_m$ which consists of the Josephson energy

$$F_J=\frac{\hbar j_c}{2e}\int_{-\infty}^{\infty}(1-\cos\varphi)dy \tag{11}$$

and the energy of magnetic fields and superconducting currents around the contact,

$$F_m=\frac{1}{8\pi}\int_{-\infty}^{\infty}\int_{-\infty}^{\infty}[\lambda^2(\nabla H)^2+H^2]dx\,dy\ . \tag{12}$$

The magnetic energy F_m can be expressed only in terms of the phase distribution $\varphi(y)$ along the defect by substituting $(\nabla H)^2=\mathrm{div}(H\nabla H)-H\nabla^2 H$ into Eq. (12). In this case the integral of $\mathrm{div}(H\nabla H)$ reduces to the vanishing integral over infinite surface enveloping the planar defect, therefore the integrand in Eq. (12) becomes $[H-\lambda^2\nabla^2 H]H$. Replacing then the term $[H-\lambda^2\nabla^2 H]$ by the right-hand side of Eq. (4), we can write F_m in the form

$$F_m=\frac{\phi_0 H(s+\xi,0)}{8\pi}+\frac{\phi_0}{16\pi^2}\int_{-\infty}^{\infty}\phi'(y)H(0,y)dy\ . \tag{13}$$

Substituting $H(0,y)$ from Eq. (7) into Eq. (13), we finally obtain

$$F_m=\left[\frac{\phi_0}{4\pi\lambda}\right]^2\left\{\ln\frac{\lambda}{\xi}+\gamma_A+\frac{1}{\pi}\int_{-\infty}^{\infty}K_0\left[\frac{\sqrt{u^2+s^2}}{\lambda}\right]\frac{\partial\varphi}{\partial u}du+\int_{-\infty}^{\infty}\frac{du}{2\pi}\int_{-\infty}^{\infty}\frac{dv}{2\pi}K_0\left[\frac{|u-v|}{\lambda}\right]\frac{\partial\varphi}{\partial u}\frac{\partial\varphi}{\partial v}\right\}\ , \tag{14}$$

where the constant $\gamma_A \approx 0.497$ takes account of the core energy.[27] At $s \gg \lambda$ the first integral in Eq. (14) vanishes, and F_m reduces to the sum of magnetic energies of the noninteracting A vortex and the planar defect, respectively.[17] At $s < \lambda$ the A vortex induces a phase distribution $\varphi(y,s)$ on the defect, with $\varphi(y,s)$ obeying Eq. (10). Notice that Eq. (10) can also be obtained from the variational principle $\delta F/\delta\varphi = 0$, where $F = F_J + F_m$, and F_J and F_m are given by Eqs. (11) and (14), respectively. The above general formulas will be used in the next sections to calculate $\varphi(y,s)$ and the pinning force $f_\perp = -\partial F/\partial s$.

B. Phase distribution

At $s \gg l$, the vortex screening current $j_\perp(s,y)$ which flows through the planar defect, is much less than j_c. In this case the nonlinear term in Eq. (10) can be linearized, $\sin\varphi \approx \varphi$, and Eq. (10) becomes a linear nonuniform integral equation which is solved in Appendix A by a Fourier transformation. This solution shows that at $s \gg l$ the planar defect is transparent for the vortex screening currents, and $\varphi(y)$ can be obtained by equating the perpendicular component $j_\perp(s,y)$ in the A vortex to the linearized Josephson current density $j_c\varphi$ [two last terms in Eq. (10), respectively]. This yields

$$\varphi(y) = -\frac{2yl}{\lambda\sqrt{s^2+y^2}} K_1\left[\frac{\sqrt{s^2+y^2}}{\lambda}\right] . \tag{15}$$

At $y^2+s^2 \ll \lambda^2$, formula (15) takes the form

$$\varphi(y) = -\frac{2yl}{s^2+y^2} . \tag{16}$$

Equations (15) and (16) correspond to the case $\varphi(y) \ll 1$ which occurs at $s \gg l$ when the planar defect weakly affects the current distribution around the A vortex. This takes place as long as the perpendicular component $j_\perp \sim c\phi_0/8\pi^2\lambda^2 s$ (Ref. 25) at the contact remains much smaller than j_c, which is equivalent to the condition $s > l$, where l is given by Eq. (2).

At $s < l$, the current distribution changes qualitatively, since the $j_\perp(s,y)$ at the contact becomes comparable to j_c. On the other hand, $j_\perp(s,y)$ cannot exceed j_c, therefore the excess current has to flow parallel to the defect. At $s \ll l$, the current density $j(s) \sim j_d\xi/s$ circulating around the vortex by the distance s from the core is much larger than j_c, so the contact behaves as a surface between the superconductor and vacuum (see below).

We now consider $\varphi(y)$ at $s \ll l$ in more detail, writing Eq. (10) in the form

$$\frac{1}{\pi}\int_{-\infty}^{\infty} \frac{\varphi'(u)}{y-u}du + \frac{2y}{s^2+y^2} + \frac{1}{l}\sin\varphi = 0 . \tag{17}$$

When deriving Eq. (17) from Eq. (10), we used the fact that at $s \ll l$ the function $\varphi'(u)$ sharply decays over lengths much shorter than λ, as will be shown below. In this case the main contribution to the integral in Eq. (10) comes from the region $|u-y| \ll \lambda$, which enables one to replace the Bessel function $K_1(x)$ by its expansion at small argument, $K_1(x) = 1/x$.

The solution of Eq. (17) should satisfy the condition $\varphi(\infty) = \varphi(-\infty) = 0$ of the conservation of magnetic flux [see Eq. (8)]. As shown in Appendix A, the ansatz

$$\varphi(y) = 2\tan^{-1}\frac{y}{s+l} - 2\tan^{-1}\frac{y}{s} \tag{18}$$

gives an asymptotically exact solution of Eq. (17) at $s \ll l$. Moreover, at $s \gg l$, Eq. (18) reduces to Eq. (16) when expanding the first arctangent in Eq. (18) in $l/s \ll 1$. Therefore, Eq. (18) provides an interpolation between the correct asymptotics of $\varphi(y)$ in two limiting cases $s \ll l$ and $s \gg l$.

Substituting Eq. (18) into Eq. (7) and integrating over y,[26] we obtain the field distribution $H(x,y)$ for $x^2+y^2 \ll \lambda^2$ in the form

$$H(x,y) = \frac{\phi_0}{4\pi\lambda^2}\left[\ln\frac{y^2+(x+s)^2}{y^2+(x-s)^2} + \ln\frac{4\lambda^2}{y^2+(x+l+s)^2} - 2C\right] , \quad x > 0 \tag{19}$$

$$H(x,y) = \frac{\phi_0}{4\pi\lambda^2}\left[\ln\frac{4\lambda^2}{y^2+(x-l-s)^2} - 2C\right] , \quad x < 0 , \tag{20}$$

where $C = 0.577$ is the Euler constant. Equations (19) and (20) allow a clear geometrical interpretation shown in Fig. 1. Namely, the field in the half-plane $x > 0$ coincides with that of the A vortex being at $x = s$, plus the field from fictitious vortex and antivortex situated at $x = -l-s$ and $x = -s$, respectively. Likewise, the field in the half-plane $x < 0$ coincides with that of a fictitious vortex being at $x = l+s$. For such a field configuration the total magnetic flux ϕ automatically equals ϕ_0 for any s.[28]

Let us now consider, what happens as the A vortex being at $x = s$ moves toward the Josephson contact. In this case its antivortex "image" being at $x = -s$ also moves toward the contact, partly compensating the field of the A vortex at $s \ll l$ (Figs. 1 and 2). As s becomes of order ξ, this vortex-antivortex pair annihilates, and the logarithmic singularity in $H(x,y)$ due to the normal core disappears. Eventually, there arises the symmetric field configuration shown in Fig. 2(c) for which $H(x,y)$ in the half-plane $x > 0$ coincides with that of a fictitious vortex being at $x = -l$, whereas the field in the half-plane $x < 0$ is determined by the fictitious vortex situated at $x = l$. It is the field distribution which corresponds to the AJ vortex localized on the planar defect.[17] The change of $j(x,y)$ and $\varphi(y,s)$ as the A vortex approaches the Josephson contact is shown in Figs. 2 and 3. Notice that the disappearance of the logarithmic singularity in $H(x,y)$ at $s \approx \xi$ results in a jumpwise (in the London theory) change of $\varphi(y,s)$ from the asymmetric distribution $\varphi(y,s)$ described by Eq. (18) to the monotonic $\varphi(y)$ described by Eq. (1). This is due to the fact that such a $A \rightarrow$AJ vortex transition occurs at the fixed magnetic flux $\phi = \phi_0$, unlike the case of a surface between superconductor and vacuum ($j_c = 0$) (Ref. 29) for which the magnetic flux in the vortex $\phi(s) = [1-\exp(-s/\lambda)]\phi_0$ decreases as it moves toward

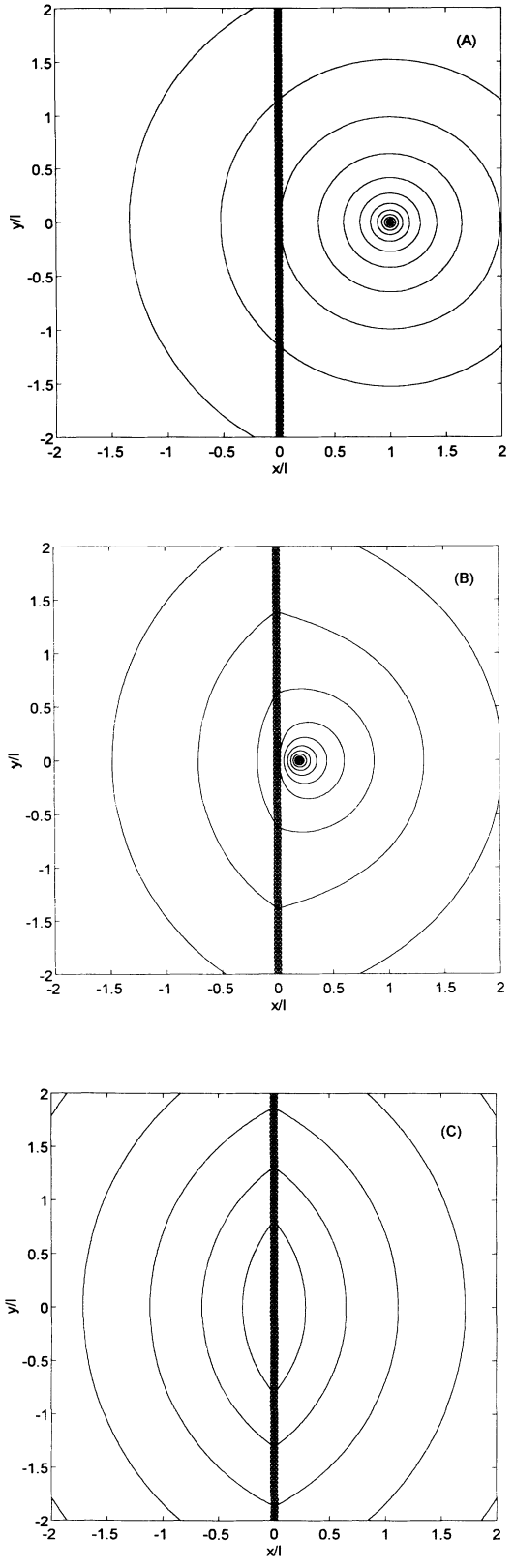

FIG. 2. Successive changes of the current distribution around the A vortex as it moves toward the planar defect. Shown are the current lines described by Eqs. (19) and (20) at $s=l$ (a), $s=0.2l$ (b), and $s=0$ (c).

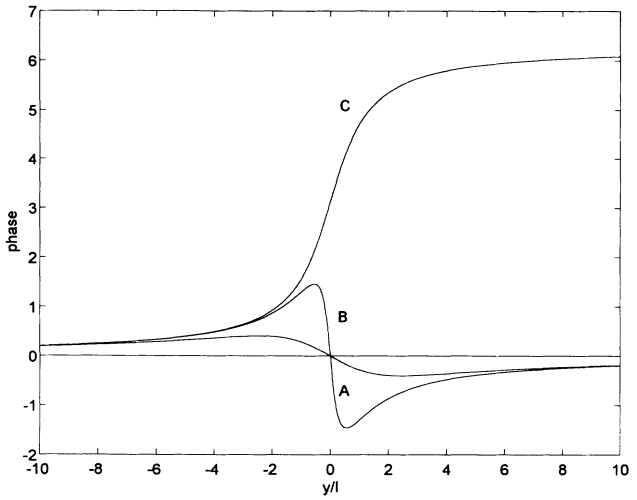

FIG. 3. The phase distributions $\varphi(y,s)$ caused by the A vortex on the planar defect at $s=l$ (a), $s=0.2l$ (b) given by Eq. (18). The curve (c) corresponds to the AJ vortex ($s=0$) described by Eq. (1).

the surface. At $j_c>0$, the second "image" vortex at $x=-l-s$ provides the closure of the transversal currents $j_\perp(y)$ flowing through the contact on the length scales of order l (Fig. 2).

III. TRANSVERSAL PINNING FORCE

To calculate the vortex energy $F(s)$ as a function of the vortex position s, we substitute Eq. (18) into Eqs. (11) and (14), which yields (see Appendix B)

$$F=\left[\frac{\phi_0}{4\pi\lambda}\right]^2\left[\ln\frac{\lambda s}{(s+l)}+\frac{l}{2s+l}+\gamma_A\right], \quad s\ll\lambda . \tag{21}$$

At $s=0$, the A vortex turns into the AJ vortex which energy is given by[17]

$$F_{\rm AJ}=\left[\frac{\phi_0}{4\pi\lambda}\right]^2\left[\ln\frac{\lambda}{l}+\gamma_{\rm AJ}\right] \tag{22}$$

with $\gamma_{\rm AJ}=0.423$. From Eqs. (2), (21), and (22), we obtain the pinning energy $F_p=F(\infty)-F_{\rm AJ}$ which decreases logarithmically as j_c increases:

$$F_p=\left[\frac{\phi_0}{4\pi\lambda}\right]^2\left[\ln\frac{j_d}{j_c}+\gamma_p\right], \tag{23}$$

where $\gamma_p=0.22$. For a uniform sample ($j_c=j_d$) the energy F_p must vanish, whereas Eq. (23) gives a nonzero, although relatively small value. This indicates that Eq. (23) cannot be used at $j_c\approx j_d$, since the NJE equations based on the assumption of uniformity of $\Delta(\mathbf{r})$, become invalid at $j_c\approx j_d$, when the variation of $\Delta(\mathbf{r})$ about the vortex core is essential.

As follows from Eqs. (21)–(23), there are two characteristic regions $\xi\ll s<l$ and $s\sim\xi$, where the interaction of the A vortex with the planar defect is determined by qualitatively different mechanisms. At $s\gg\xi$, the defect

does not affect the normal core of the A vortex which is attracted to the defect mostly due to the long-range magnetic interaction. As the distance s becomes comparable with ξ, the normal core turns into the AJ phase core, so the gain of the condensation energy $\delta F=F(\xi)-F_{\rm AJ}$ can be regarded as the core pinning energy which can be calculated from Eqs. (21) and (22) as follows:

$$\delta F=\gamma_c\left[\frac{\phi_0}{4\pi\lambda}\right]^2, \tag{24}$$

where $\gamma_c=1+\gamma_A-\gamma_{\rm AJ}=1.07$. At $s\gg\xi$, the pinning force $f_\perp=-\partial F/\partial s$ is given by

$$f_\perp(s)=-l\left[\frac{\phi_0}{4\pi\lambda}\right]^2\left[\frac{1}{s(s+l)}-\frac{2}{(2s+l)^2}\right], \tag{25}$$

where the first and the second terms in the square brackets result from the magnetic and the Josephson parts of F, respectively. In two limiting cases, formula (25) yields,

$$f_\perp(s)=-\frac{l}{2s^2}\left[\frac{\phi_0}{4\pi\lambda}\right]^2, \quad l\ll s<\lambda \tag{26}$$

$$f_\perp(s)=-\frac{1}{s}\left[\frac{\phi_0}{4\pi\lambda}\right]^2, \quad \xi<s\ll l\ . \tag{27}$$

At $s\ll l$ the interaction force $f_\perp(s)$ is independent of j_c and turns out to be equal to the attraction force between the vortex and the planar sample surface.[29] This is due to the fact that at $s\ll l$ only a small part of $j(\mathbf{r})$ in the vortex can pass through the contact which effectively behaves as a surface with $j_c=0$. In terms of the field configuration shown in Figs. 1 and 2, the main contribution to $f_\perp(s)$ at $s\ll l$ comes from the interaction of the A vortex with the nearest image antivortex being at $x=-s$. By contrast, at $s\gg l$ the planar defect weakly disturbs the current flow around the vortex, which results in a significant drop of the interaction force $f_\perp(s)$ as compared to the pure magnetic force (27). At $s>l$, the contact becomes transparent for $\mathbf{j}(s,y)$ induced by the A vortex at $x=s$, and $f_\perp(s)$ can exhibit two different behaviors, depending on the ratio j_c/j_l. In the nonlocal regime $j_l<j_c<j_d$, the force $f_\perp(s)$ given by Eq. (26) turns out to be inversely proportional to j_c and decreases as $1/s^2$ at $l<s<\lambda$. For $s>\lambda$, both $f_\perp(s)\propto\exp(-s/\lambda)$ and $\varphi(y,s)$ exponentially decrease with s [see Eq. (15)]. In the local regime, $j_c<j_l$, the force $f_\perp(s)$ is described by Eq. (27) at $s<\lambda$ and decreases exponentially with s at $s>\lambda$. Therefore the strong magnetic pinning virtually occurs only within the layer of thickness $\sim l\approx\xi j_d/j_c$ around the planar defect. Notice that although $H(x,y)$ at the planar defect coincides with the field produced by the vortex-antivortex images shown in Fig. 1, the interaction force $f_\perp(s)$ *is not equal* to the force between the A vortex being at $x=s$ and the image vortex-antivortex pair at $x<0$. This is due to the integral term in Eq. (13), unlike the well-known case of the vortex at the surface between superconductor and vacuum[29] for which that term vanishes.

At $s\sim\xi$, the pinning force $f_\perp\approx\delta F/\xi$ is also due to the change of the vortex core structure. Using Eq. (24), we obtain the value of $f_\perp$ which is of the order of the magnetic force given by Eq. (27) at $s\sim\xi$:

$$f_\perp\simeq\frac{\gamma_c}{\xi}\left[\frac{\phi_0}{4\pi\lambda}\right]^2. \tag{28}$$

Therefore $f_\perp(s)$ is determined by the long-range magnetic forces at $\xi\ll s<l$ and by short-range core interaction at $s\sim\xi$.

IV. LONGITUDINAL PINNING FORCE

Pinning force, $f_\parallel$, along the planar defect qualitatively differs from the perpendicular component $f_\perp$, since for the homogeneous planar defect $f_\parallel$ vanishes, and the nonzero $f_\parallel$ results from the pinning of AJ vortices by inhomogeneities of $j_c(y)$ due to variations of thickness or chemical composition, dislocation network, etc. (see, e.g., Refs. 10 and 11). Additionally, an AJ vortex interacts with pinned neighboring A vortices, which gives rise to a collective contribution to $f_\parallel$. These components are considered separately by taking $f_\parallel=f_1+f_2$, where f_1 results from inhomogeneities of $j_c(\mathbf{r})$, and f_2 is due to the magnetic interaction of the AJ vortex with pinned intragrain A fluxons (Fig. 4).

The value f_1 can be estimated by calculating the characteristic gain in the core energy δF_J of the AJ vortex as it is moved from a nonuniformity of length $\sim L$ along the planar defect.[30,31] For the phase AJ core the pinning force $f(u)$ is due to a gradient of the Josephson energy density $\hbar j_c(y)/e$:

$$f(u)=-\frac{\hbar}{e}\frac{\partial}{\partial u}\int_{-\infty}^{\infty}j_c(y)\sin^2\frac{1}{2}\varphi(y-u)\,dy\ , \tag{29}$$

where u is a displacement of the vortex center from an equilibrium pinning position, J_c being determined by the maximum value of $f(u)$. In general, $\varphi(y)$ should be calculated self-consistently from Eq. (10) with nonuniform

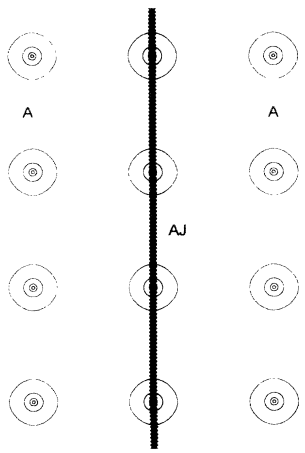

FIG. 4. Interplay between intragrain A vortices and intergrain AJ vortices. The preferential motion of AJ vortices along the planar defects is prevented by inhomogeneities of $j_c(\mathbf{r})$ and the local energy barriers caused by the fields of pinned neighboring A fluxons.

$j_c(y)$, however here we restrict ourselves to characteristic limiting cases for which $f(u)$ can be obtained without solving Eq. (10).

First we consider a smooth inhomogeneity in which $j_c(y)$ changes over the length L much larger than the core size l. In this case $\varphi(y)$ is determined by local value of $j_c(y)$ at the vortex center $y=u$, so one can use Eqs. (1) and (2) in which $l(y)$ changes weakly over the length $\sim l[lj_c'(u)\ll j_c(u)]$. Differentiating Eq. (29) and changing the variable $y=y+u$, one obtains

$$f(u)=-\frac{\hbar}{2e}\int_{-\infty}^{\infty} j_c(y+u)\sin\varphi(y)\frac{\partial\varphi(y)}{\partial y}dy$$
$$=-\frac{\hbar}{2e}\int_{-\infty}^{\infty}[j_c(u)+yj_c'(u)]\frac{4l^2y}{(y^2+l^2)^2}dy\ . \qquad (30)$$

Here the term $\sin\varphi(y)d\varphi/dy$ was transformed by means of Eq. (1), and the slowly changing function $j_c(y)$ was expanded about the point $y=0$. The contribution from the first term in the square brackets in Eq. (30) vanishes, and the second term gives the force $f(u)$ proportional to the local gradient $j_c'(u)$. Performing the integration in Eq. (30), we finally obtain

$$f(u)=-\frac{\phi_0 l}{c}\frac{\partial j_c(u)}{\partial u}\ . \qquad (31)$$

Now we calculate $f(u)$ for the opposite case of point inhomogeneity ($L\ll l$) for which one can substitute $j_c(y+u)=j_{c0}+\Gamma\delta(y+u)$ in Eq. (30). Here

$$\Gamma=\int_{-\infty}^{\infty}[j_c(y)-j_{c0}]dy=L\delta j_c\ , \qquad (32)$$

where δj_c is a characteristic amplitude of local $j_c(y)$ variations around the mean value j_{c0}. Then

$$f(u)=-\frac{\hbar\Gamma}{2e}\sin\varphi(u)\frac{\partial\varphi(u)}{\partial u}\ . \qquad (33)$$

We consider here the case of weak inhomogeneity ($L\delta j_c\ll lj_{c0}$) for which $f(u)$ can be calculated in first order in $\Gamma\ll 1$. This allows one to neglect the corrections of order Γ in $\varphi(y)$ and substitute Eq. (1) into Eq. (33). This yields the following equation for the vortex displacement $u(f)$ as a function of the driving force $f=\phi_0 j/c$:

$$f=\frac{2\hbar\Gamma}{e}\frac{l^2u}{(l^2+u^2)^2}\ . \qquad (34)$$

The function $f(u)$ attains the maximum at $u_m=l/\sqrt{3}$, so the pinning force $f_1=f(u_m)$ is

$$f_1=\frac{3\sqrt{3}\Gamma\phi_0}{4cl}\ . \qquad (35)$$

Therefore, the dependence of f_1 on the characteristic size of inhomogeneity L can be summarized as follows. At small $L(L\ll l)$ the force f_1 is proportional to the parameter Γ which linearly increases with L [see Eq. (32)]. At large $L(L\gg l)$ the value f_1 is proportional to the gradient $j_c'(u)\sim\delta j_c/L$, so f_1 decreases as $1/L$. Therefore, $f_1(L)$ is maximum if L becomes of the order of the core size l.

In general, the pinning potential $U(y)=\hbar j_c(y)/e$ may be considered as consisting of different inhomogeneities with distributions of amplitudes δj_c, sizes L, and positions. For a qualitative description of this case, one can use the above result for single inhomogeneities, if a characteristic size of inhomogeneities L is much smaller than l, and the spacing between them is larger than l. Then AJ vortices virtually interact with isolated inhomogeneities for which the pinning force f_1 is proportional to L [see Eqs. (32) and (35)]. Using Eqs. (2) and (32), one can write Eq. (35) in the form $f_1\sim\alpha(\phi_0/4\pi\lambda)^2L/l^2$, where $\alpha=\delta j_c/j_{c0}$ is a dimensionless parameter which characterizes the degree of inhomogeneity along the planar defect. Likewise, for $L\gg l$, one obtains from Eq. (31) that $f_1\sim\alpha(\phi_0/4\pi\lambda)^2/L$ is inversely proportional to L. Both cases $L\gg l$ and $L\ll l$ can be described by the interpolation formula

$$f_1\simeq\alpha\left[\frac{\phi_0}{4\pi\lambda}\right]^2\frac{L}{L^2+l^2}\ , \qquad (36)$$

which shows that the force $f_1(L)$ attains the maximum when L becomes of the order of the core size l. In the case of a wide distribution of L, a mean pinning force $\langle f_1\rangle$ can be obtained by averaging Eq. (36) with the corresponding distribution function $G(L)$.

To calculate the magnetic contribution f_2, we suppose that the vortex structure consists of intragrain A fluxons having normal cores of radius $\sim\xi$ and the AJ vortices localized on the planar defects. The substantial difference in their core sizes (ξ and l, respectively) implies that the AJ vortices, in general, are pinned much weaker than A fluxons. For example, if both pinning potentials $U(\mathbf{r})$ for A and AJ vortices vary over the same scale $L\sim\xi$, the pinning of A vortices is most effective, while AJ vortices are pinned much weaker, since their core size l is much larger than L. Such a mismatch of the $U(\mathbf{r})$ for AJ and A fluxons results in a large difference in their elementary pinning forces f_A and f_{AJ}, respectively. In particular, Eq. (36) yields $f_{AJ}\sim(\xi/l)^2f_A\sim(j_c/j_d)^2f_A\ll f_A$. However even if $U(\mathbf{r})$ is optimized for both types of vortices simultaneously [$U_A(\mathbf{r})$ within the grains varies over lengths $\sim\xi$, whereas $U_{AJ}(\mathbf{r})$ varies along the grain boundaries over lengths $\sim l$], the force f_{AJ} still remains much smaller than f_A, namely, $f_{AJ}\sim(j_c/j_d)f_A\ll f_A$. Therefore the inequality $f_{AJ}\ll f_A$ holds for most typical situations, except the special case of weak bulk pinning of A fluxons for which f_A may be smaller or of order f_{AJ}.

Hence it follows, that the longitudinal core pinning of AJ fluxons is weaker than that of intragrain A fluxons, so the planar defect can become a channel for the preferential flux motion.[17] This, in turn, gives rise to an additional magnetic pinning of AJ vortices as they are driven through the strongly pinned A vortices (Fig. 4). We estimate this contribution, f_2, to $f_\parallel$ for $H_{c1}\ll H\ll H_d$, where H_{c1} and H_{c2} are the lower and upper critical fields, respectively, and $H_d\sim\phi_0/l^2$. Above H_d, the AJ cores overlap, breaking the phase coherence across the grain boundary and resulting in the superconducting decoupling of the grains. Using Eq. (1), one can write H_d in the

form

$$H_d=\frac{1}{\phi_0}\left[\frac{16\pi^2\lambda^2 j_c}{c}\right]^2\simeq\left[\frac{j_c}{j_d}\right]^2 H_{c2}\ . \tag{37}$$

At $H<H_d$ the spacing between vortices, $a=(\phi_0/H)^{1/2}$, is larger than l, and the difference between the core structures of AJ and A vortices does not affect their magnetic interaction which remains the same as the well-known A-A vortex interaction.[25] The force f_2 equals the maximum gradient of the vortex magnetic energy along the defect, $f_2=-\nabla\phi_0\delta H(\mathbf{r})/4\pi$, where $\delta H(\mathbf{r})$ is the quasiperiodic fluctuation of the local field $H(\mathbf{r})$ in the flux-line structure around the mean value H. Since $\delta H(y)$ changes over the intervortex spacing a, the force f_2 can be estimated as $f_2\approx\phi_0\langle\delta H^2\rangle^{1/2}/4\pi a$, where $\langle\delta H^2\rangle$ is the mean-squared dispersion of $\delta H(\mathbf{r})$. Then using the formula $\langle\delta H^2\rangle=\phi_0^2/16\pi^3\lambda^4$ valid for $H_{c1}\ll H\ll H_{c2}$,[32] and combining both contribution f_1 and f_2, we obtain

$$f_\parallel\simeq\left[\frac{\phi_0}{4\pi\lambda}\right]^2\left[\frac{\alpha L}{L^2+l^2}+\sqrt{H/\pi\phi_0}\right]\ . \tag{38}$$

As follows from Eqs. (27) and (38), there is a substantial difference between the transversal and longitudinal components $f_\perp$ and $f_\parallel$. For instance, the value $f_\perp(s)$ attains the maximum at $s\approx\xi$, where

$$f_\perp^{\max}\simeq\frac{\gamma_c}{\xi}\left[\frac{\phi_0}{4\pi\lambda}\right]^2\sim\frac{j_d\phi_0}{c}\ . \tag{39}$$

By contrast,

$$f_\parallel\sim\frac{j_d\phi_0}{c}\left[\frac{\sqrt{2}\pi a\xi L}{L^2+l^2}+\sqrt{H/H_{c2}}\right]\ , \tag{40}$$

where $H_{c2}=\phi_0/2\pi\xi^2$. Hence it follows that at $H\ll H_{c2}$, the inequality $f_\perp^{\max}\gg f_\parallel$ holds for any L, since $l\gg\xi$. The strong anisotropy of f results from the weak-link properties of the planar defect and takes place for any interface with $j_c\ll j_d$. Notice that $f_\parallel(H)$ increases with H, the degree of anisotropy $f_\parallel/f_\perp^{\max}$ decreasing as H increases. The field H_s above which $f_\parallel$ is mostly determined by the shear flux pinning, can be obtained by equating two terms in the square brackets in Eq. (38), which yields

$$H_s=\frac{\pi\alpha^2L^2\phi_0}{(L^2+l^2)^2}\ . \tag{41}$$

The function $H_s(L)$ attains the maximum $H_s^{\max}=\alpha^2\phi_0\pi/4l^2=0.8\alpha^2H_d$ at $L=l$. Since $\alpha<1$, the value H_s is always less than the decoupling field H_d above which the AJ phase cores overlap. Here H_s decreases as the parameter $\alpha=\delta j_c/\langle j_c\rangle$ decreases and can be much smaller than H_d, especially if $L\gg l$, or $L\ll l$. In this case there is a wide field region $H_s\ll H\ll H_d$, where $f_\parallel(H)$ increases with H as $H^{1/2}$. Notice that at $H_s\ll H\ll H_d$, the first term in the square brackets in Eq. (40) can be neglected, and $f_\parallel$ becomes independent of the properties of planar defect.

V. PINNING IN A RANDOM NETWORK

A. Critical current

Now we consider qualitative features of the flux pinning in a network of planar high-j_c defects, assuming a mean grain size D to be much larger than l (Fig. 5). In this case the grain boundary component of the flux pinning is mostly determined by a small fraction of vortices being within the effective layer of thickness $\sim l\approx\xi j_d/j_c$ bordered the planar defects. At low fields $H<H_d$, the spacing between fluxons is larger than l, therefore this pinning layer contains only AJ vortices whose phase cores do not overlap. Here we consider two characteristic cases shown in Fig. 5, namely a system of mutually connected grains (A) and a random network of planar defects (B) which may model the α-Ti ribbons in optimized Nb-Ti.[1]

In this paper we restrict ourselves to the more clear two-dimensional (2D) case which pertains to thin films in transversal field, optimized Nb-Ti with α-Ti ribbons parallel to **H**, or layered HTS's (especially Bi or Tl-based HTS's) if **H** is parallel to the c axis, etc. As follows from the above results, each planar defect in Fig. 5, acts as a strong pin in the direction perpendicular to its plane, whereas the longitudinal pinning force $f_\parallel$ is much smaller than $f_\perp$. If the defect concentration exceeds the percolation threshold, the network can provide channels for the

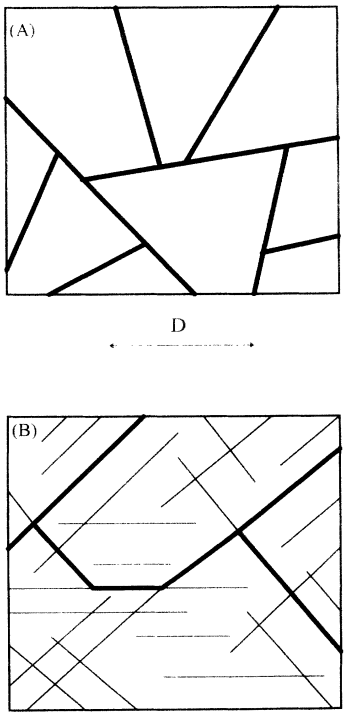

FIG. 5. Examples of the 2D pinning networks: structure of mutually connected grain boundaries (a), random network of planar defects (b). Bold lines show the defects which form the percolative channels for the preferential motion of AJ vortices. Thin lines in (b) correspond to the "dead ends" and isolated defects which do not belong to the percolation paths.

preferential motion of AJ vortices along continuous paths which connect the opposite sides of the sample. In the case shown in Fig. 5(a), these paths just comprise the whole grain-boundary surface. For the random network shown in Fig. 5(b), the situation is more complicated. Indeed, as known from the percolation theory,[20] such a network has a very complex topological structure, mostly consisting of isolated defects or the defects which are connected to the net, but do not belong to the percolative paths. These so-called "dead ends"[20] do not contribute to the percolative flux motion, but rather act as additional pinning centers for vortices being between the flux channels. As a result, J_c can be limited by the percolative channels with minimum $f_\parallel$. Notice that the flux channels caused by local shear distortions in the vortex structure have been discussed in the literature.[33–37] However, unlike the weakly pinned single rows of AJ vortices discussed in this paper, those channels of local plastic flux flow were considered without taking account of the change of the core structure at the planar defects. Similar channels have also been discovered in the 2D computer simulations of A vortices pinned by randomly distributed point defects[38] and J vortices in disordered Josephson junction arrays.[39] The 3D network does not allow the clear geometrical interpretation shown in Fig. 5, since now each vortex crosses several grains, and the percolative motion of vortex segments along randomly oriented planar defects can require strong tilt distortions of flux lines.[40,41]

We consider here two characteristic regimes for which J_c is limited by the parallel and perpendicular components of $\mathbf{f}$, respectively. The first one corresponds to the strong intragrain pinning ($U_A \gg U_{AJ}$) for which the AJ vortices on the planar defects are pinned much weaker than the intragrain A vortices owing to the large difference in their core sizes and the mismatch of inter- and intragrain pinning potentials. As a result, J_c is determined by weakly pinned AJ vortex rows along the percolative paths. The critical current density, J_c can be obtained from the balance of the Lorentz and pinning forces, $\phi_0 J_c/c \simeq G f_\parallel$, where $f_\parallel$ is given by Eq. (38), and $G \sim 1$ is a geometrical factor which depends on the shape of the vortex channel and its orientations with respect to the current direction. Hence,

$$J_c(H) = [1+\sqrt{H/H_s}]J_0 \ , \quad H_{c1} \ll H < H_d \tag{42}$$

$$J_0 \simeq \frac{c\phi_0 \alpha L G}{16\pi^2\lambda^2(L^2+l^2)} \ . \tag{43}$$

The characteristic feature of this case is the *increase* of $J_c(H)$ with H due to the magnetic forces caused by strongly pinned intragrain A vortices. At $H > H_s$ this mechanism dominates, and $J_c(H)$ becomes independent of the properties of planar defects:

$$J_c \simeq \frac{cG\sqrt{\phi_0 H}}{16\pi^{5/2}\lambda^2} \ . \tag{44}$$

The amplitude J_0 is independent of j_c at $L \gg l$ and proportional to $1/l^2 \propto j_c^2$ at $L \ll l$.

For the random network shown in Fig. 5(b), only a small part of defects belongs to the percolative path, and the AJ vortices localized on isolated defects or "dead ends" do not affect the macroscopic J_c. Those parts of the pinning network give rise to an additional pinning of A vortices in the directions perpendicular to the planar defects. Furthermore, AJ vortices can be depinned from the edges of planar defects and thereby turned into intragrain A vortices. This requires the depinning force $f_\parallel = f_1 + f_2$, where $f_1 \sim \phi_0 j_c/c = (\phi_0/4\pi\lambda)^2/l$, and $f_2 \sim \phi_0 \langle \delta H^2 \rangle^{1/2}/4\pi a$. However, such a process only results in a local flux redistribution at the defect edges, since the A vortex depinned from the defect edge experiences much stronger bulk pinning than the AJ vortices on the percolative path.

Now we discuss the opposite case of weak intragrain pinning for which J_c is mostly due to flux pinning by grain boundaries. For the sake of simplicity we do not consider here the random network, restricting ourselves to the more clear case shown in Fig. 5(a) for which the total Lorentz force $f_L \sim D^2 J_c H/c$ acting on the unit length of A fluxons within the grain of size D, is to be balanced by the pinning force $\mathbf{f}$ integrated over the total surface of grain boundary. Since $\mathbf{f}$ is highly anisotropic with respect to $\mathbf{J}$, we can neglect the small parallel component $f_\parallel$ as compared to $f_\perp$ and calculate the total pinning force per grain, f_p, by averaging the transversal elementary pinning force $f_\perp^{\max}$ over the grain surface S,

$$f_p = \left[\frac{B}{\phi_0}\right]^{1/2} f_\perp^{\max} \oint_s \cos\theta(\mathbf{r}) dS \tag{45}$$

where $(H/\phi_0)^{1/2}$ is the linear density of AJ vortices, and $\theta(\mathbf{r})$ is the angle between the direction of the Lorentz force and the local normal to the grain-boundary surface. The parallel components of $\mathbf{f}$ are to be balanced by shear stresses in the vortex structure. Equating f_p to Lorentz force $f_L = HVJ/c$ acting on the vortices within the grain of volume V, we obtain J_c in the form

$$J_c = \frac{c\phi_0\gamma_c}{16\pi^2\lambda^2\xi D}\sqrt{\phi_0/H} \sim j_d \frac{\xi}{D}\sqrt{H_{c2}/H} \ , \tag{46}$$

where the effective grain size D is determined by

$$\frac{1}{D} = \frac{1}{V}\oint_s \cos\theta(\mathbf{r}) dS \ . \tag{47}$$

Here J_c is inversely proportional to D and behaves as $H^{-1/2}$ at $H \ll H_{c2}$, which is characteristic for the grain-boundary pinning.[2,30] The $1/D$ dependence of J_c holds as long as $D > l$. Notice that due to the presence of $\cos\theta$ in Eq. (47), the length D depends on both the grain shape, and the orientation of $\mathbf{J}$. In particular, for a thin rectangular grain of width D_1 and of thickness $D_2 \ll D_1$, the value D equals either D_1 or D_2, if $\mathbf{J}$ flows parallel or perpendicular to the smallest grain side, respectively.

Therefore, the relationship between the intra- and intergrain pinning forces can significantly affect the field dependence of J_c. In the case of weak intragrain pinning, $J_c(H)$ is determined by the transversal component $f_\perp$ and monotonically decreases with H. By contrast, if the intragrain pinning dominates, J_c is mostly determined by

weakly pinned AJ vortices along the percolation paths formed by the grain boundaries for which $f_{\parallel}(H)$ increases with H. This can give rise to a nonmonotonic field dependence of $J_c(H)$: at small H, $J_c(H)$ increases up to the field above which the J_c determined by pinning along the planar defects becomes comparable with J_c due to bulk intragrain pinning. At higher fields, $H > H_p$ the planar defects cease to be the easy flux-flow channels, and J_c is determined by the collective intragrain pinning which gives rise to a decrease of $J_c(H)$ with H. The appearance of such a nonmonotonic dependence of $J_c(H)$ due to a crossover between these two pinning mechanisms is shown in Fig. 6.

B. Magnetic granularity

As was mentioned in the Introduction, flux pinning determines J_c provided that $j_c > J_c$, so the pinning structure does not block the current flow. Otherwise the current-carrying capacity is limited by j_c of planar defects, since at $j_c < J_c$ only a small part of the superconducting currents circulating within grains can pass through the grain boundaries. This gives rise to the magnetic granularity (MG) due to the appearance of intragrain current loops.

In certain regions of T and H, the MG can occur even for high-j_c planar defects if J_c and j_c strongly depend on T and H. As a model of the high-j_c defects, we consider strongly proximity coupled S-N-S Josephson contacts for which the exponential field dependence $j_c = j_0 \exp(-H/H_0)$ was observed.[42-44] Here H_0 is a characteristic decoupling field which depends on the parameters of the normal layer and increases as the thickness of the contact d decreases. The amplitude $j_0 = j_m \exp(-d/\xi_n)$ strongly depends on both d and T as well, where the $\xi_n = \hbar v_F / 2\pi k_B T$ is the proximity length, and v_F is the Fermi velocity[45] (we consider here the clean limit $l_i > \xi_n$, where l_i is the electron mean free path). In this case the MG condition $j_c(T,H) < J_c(T,H)$ can be written as follows:

$$\frac{T}{T_0} + \frac{H}{H_0} > \ln \frac{j_m}{J_c} . \tag{48}$$

Here $T_0 = \hbar v_F / 2\pi k_B d$ is a decoupling temperature. As seen from Eq. (48), the MG tends to arise at high T and H, the details of temperature and field dependences of J_c manifesting themselves only via the logarithmic term in Eq. (48) weakly affecting MG condition.

A similar situation may occur at low H as well, for example, if the grain-boundary pinning dominates and $J_c(H) \propto H^{-1/2}$ [see Eq. (46)]. Then the inequality $J_c(H) > j_c$ holds if

$$H < H_g = \frac{H_{c2}}{\ln^2(\beta D/l)} , \tag{49}$$

where $\beta \sim 1$. At $D/l = 10-100$, the value H_g can be comparable to H_{c1} for typical type-II high-J_c superconductors such as Nb-Ti ($\kappa \approx 40$), etc.

Notice that the nonmonotonic dependence of $J_c(H)$ shown in Fig. 6 could also be regarded as a manifestation of MG. Indeed, the interpretation of this regime proposed in this paper implies a strong intragrain pinning at low fields, whereas J_c is mostly determined by much weaker pinning of AJ vortices along the percolative paths formed by planar defects. This can give rise to the appearance of closed current loops within the grains, where the local critical current densities can be larger than the macroscopic J_c.

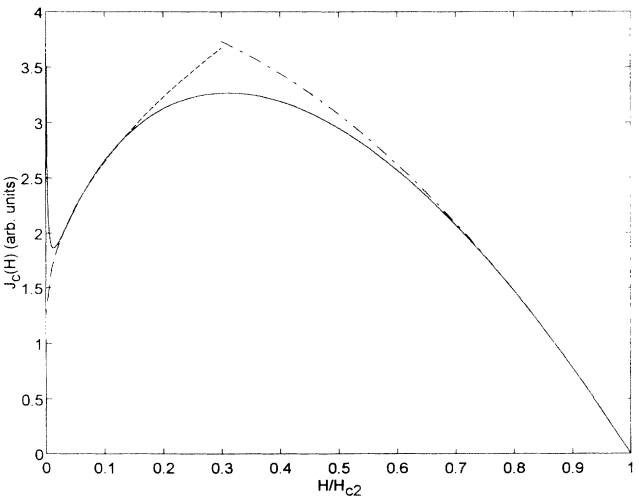

FIG. 6. A mechanism of the nonmonotonic field dependence of $J_c(H)$ due to the crossover between the inter- and intragrain pinning mechanisms. At small H, the value of J_c is limited by the weak pinning of AJ vortices along the percolative channels [dashed curve described by Eq. (42)]. In the high-field region the limiting mechanism becomes the collective bulk pinning (dot-dashed curve obtained without account of the percolation effects).

VI. DISCUSSION

In this paper we consider flux pinning by planar high-j_c defects with $j_c > J_c$ which do not cause a pronounced MG, but rather play the role of "hidden" weak links which qualitatively change the normal cores of A fluxons. We calculated the elementary pinning force $\mathbf{f}(s)$ due to interaction of A vortices with high-j_c planar Josephson contacts. The maximum in the transversal component $f_{\perp}(s)$ corresponds to $s \approx \xi$ when the intragrain A vortex with normal core turns into the intergrain AJ vortex with the phase core which is a 2π phase kink of length $l \gg \xi$ along the contact and of width $\sim \xi$ in the transversal direction. Such an anisotropy of the phase AJ core manifests itself in a strong anisotropy of $\mathbf{f}(s)$ with respect to the orientation of $\mathbf{J}$ to the contact plane, the maximum and the minimum in $\mathbf{f}$ corresponding to $\mathbf{J}$ parallel and perpendicular to the contact, respectively. This can give rise to percolative channels for preferential motion of AJ vortices which determine J_c in the 2D case. The pinning force $f_{\parallel}$ along the percolative path is determined by both local inhomogeneities of $j_c(\mathbf{r})$ of planar de-

fects and the magnetic interaction of AJ vortices with strongly pinned intragrain A vortices. The second contribution results in the increase of $f_{\parallel} \propto H^{1/2}$ at $H > H_s$.

Notice that our conclusion on the reduced flux pinning along planar defects was made by means of the analysis of the elementary pinning forces taking account of neither elastic properties of fluxons, nor thermal fluctuations of vortex positions. For instance, in the collective pinning model,[40] strong thermal fluctuations could *increase* J_c parallel to the planar defects, which may pertain to the observed decrease of the resistivity along twins in HTS's.[7,8] On the other hand, direct magneto-optical images of the flux penetration into HTS single crystals[46,47] have shown a preferential vortex motion along twins, which is consistent with our result on the reduced longitudinal pinning force $f_{\parallel}$ as compared to $f_{\perp}$. A possible explanation of this apparent contradiction may be due to the fact that those opposite behaviors correspond to different regions of T and B, namely the magneto-optic experiments were done at low T and B, well below the irreversibility line, whereas the resistive measurements were performed at high T and B, above the irreversibility line. For instance, in the model proposed in this paper, the flux channels exist only at low fields and temperatures, where J_c is due to the single-vortex pinning along the planar defects, and thermal fluctuations are negligible (see Fig. 6). However, the increase of $f_{\parallel}$ with H gives rise to a crossover from the single-vortex to collective pinning regime at higher T and H for which J_c is determined by both intragrain bulk pinning and the averaged transversal component $f_{\perp}$. In this case J_c along the twins may become *larger* than the macroscopic J_c due to the dimensional suppression of thermal fluctuations of AJ vortices on the planar defects as compared to the intragrain A vortices.[40] This also correlates with magneto-optic measurements on twinned and detwinned $YBa_2Cu_3O_7$ single crystals[48] which do show a significant increase of contribution of twins to J_c above 45 K.

Planar high-j_c crystalline defects can provide strong transversal flux pinning resulting in J_c which depends weakly on the properties of the pins in the absence of magnetic granularity ($j_c > J_c$). At the same time, the topology of the pinning network can play a very important role, because J_c can be limited by the shear flux pinning along the percolative paths formed by a small fraction of defects. Here the increase of the longitudinal pinning force $f_{\parallel}$ can result in the nonmonotonic dependence $J_c(B)$ due to a crossover between inter- and intragrain pinning mechanisms (Fig. 6). This may pertain to the nonmonotonic field dependence of $J_c(H)$ observed both on LTS's (Refs. 49 and 50) and HTS's (Refs. 14, and 51–58) (the so-called "fishtail" effect), which has been interpreted in the literature in terms of a field-induced decoupling of superconducting grains,[6,49–52] percolation effects,[53–55] flux creep,[56–58] dimensional crossover in the collective pinning model,[59] etc. It should be emphasized that the value J_c given by Eqs. (44) at $H \gg H_c$ turns out to be independent of the microscopic parameters of planar defects which only provide the channels for the preferential flux motion. Therefore, the increase of $J_c(H)$ with H may occur for any percolative network of weakly pinned single-vortex rows, in particular, for the "grain boundaries" in the 2D flux-line lattice caused by randomly distributed point pinning centers studied numerically in Ref. 38. Another distinctive feature is the inverse dependence of J_c on the characteristic grain size, D. The dependence $J_c \propto 1/D$ is characteristic for the pinning due to grain boundaries[30] and was observed, for example, in Nb_3Sn (Ref. 2) and Chevrel phases.[3,4]

In the case of strong grain-boundary pinning, $J_c(b)$ displays the characteristic low-field dependence $J_c(b) \propto b^{-1/2}$ which is specific for flux pinning by planar defects.[30] Such a behavior is consistent with the dependence $J_c(b) = J_0 b^{-1/2}(1-b)^{\beta}$ often observed on both LTS's (Refs. 30 and 60) and HTS's, in particular, on $YBa_2Cu_3O_7$,[61] $Bi_2Sr_2CaCu_2O_x$,[62,63] $Bi_2Sr_2Ca_2Cu_3O_x$,[62] $HgBa_2CuO_{4+x}$,[64] where $1 < \beta < 2$, $b = B/B_*$, and $B_*(T)$ is the irreversibility field. However, at high fields $H > H_g$ the critical current may be determined by j_c of the pinning network rather than the flux pinning. Such a granularity transition can manifest itself in the change of $J_c(H)$ dependences above the decoupling field H_g. For instance, in the case of proximity-coupled normal layers for which $j_c = j_m \exp(-H/H_0)$, this can give rise to an exponential field dependence of $J_c(H)$ at $H > H_g$. A similar dependence of $J_c(H)$ was indeed observed on optimized Nb-Ti superconductors with artificial pinning centers.[60]

The preferential vortex motion along the percolative network can also strongly affect flux dynamics and current-voltage characteristics,[17,36–40] changing the dependence of the flux creep rate on T and H as compared to the uniform flux motion. In particular, this can result in the increase of the apparent flux-creep activation energy with temperature due to the change of the effective number of percolative channels with T.[36]

ACKNOWLEDGMENTS

We are grateful to D.C. Larbalestier for useful discussions. This work was supported by Department of Energy–Division of High Energy Physics and NSF Materials Research Group Program (DMR 9214707).

APPENDIX A: SOLUTION OF EQ. (10)

We first consider the case $s \gg l$. Then $\sin\varphi \approx \varphi$, and Eq. (10) becomes

$$\int_{-\infty}^{\infty} \varphi''(u) K_0\left[\frac{|y-u|}{\lambda}\right]\frac{du}{\pi} - \frac{\varphi(y)}{l} = \frac{2y}{\lambda\sqrt{s^2+y^2}} K_1\left[\frac{\sqrt{s^2+y^2}}{\lambda}\right]. \quad \text{(A1)}$$

Equation (A1) can be solved by the Fourier transformation, which yields (see, e.g., Ref. 26)

$$\left[\frac{k^2\lambda^2}{\sqrt{1+k^2\lambda^2}} + \beta\right]\varphi_k = -\frac{2\pi i\lambda \exp[-s\sqrt{k^2+\lambda^{-2}}]}{\sqrt{1+k^2\lambda^2}}, \quad \text{(A2)}$$

where φ_k is the Fourier transform of $\varphi(y)$, and $\beta = \lambda/l$. Performing the inverse Fourier transformation of φ_k, one

can present $\varphi(y)$ in the form

$$\varphi(\rho)=\int_{-\infty}^{\infty}\frac{q\sin(q\rho)\exp[-(s/\lambda)\sqrt{1+q^2}]dq}{q^2+\beta\sqrt{1+q^2}} \tag{A3}$$

with $\rho=y/\lambda$ and $q=k\lambda$. At $s\ll\lambda$, the main contribution to the integral (A3) comes from $q\gg1$, therefore one can replace $(1+q^2)^{1/2}=|q|$ and express Eq. (A3) via the exponential integral function $Ei(z)$ (Ref. 26) as follows:

$$\varphi(y)=-2\,\mathrm{Im}\exp\frac{(s-iy)}{l}Ei\left[-\frac{(s-iy)}{l}\right] . \tag{A4}$$

The condition $\varphi(y,s)\ll1$ is equivalent to $s\gg l$, so we should use the asymptotic expansion of $Ei(-z)=\exp(-z)[1+1/z+\cdots]$ at $|z|\gg1$.[26] Then Eq. (A4) reduces to Eq. (16). On the other hand, in the nonlocal regime ($\beta=\lambda/l\gg1$) one can neglect the term q^2 in the denominator of Eq. (A3), which, according to Eq. (A2), is equivalent to the neglecting of the integral in Eq. (A1). Then the evaluation of the integral in Eq. (A3) (Ref. 26) results in Eq. (15).

Now we consider the case $s\ll l$ and look for the solution of Eq. (17) in the form

$$\varphi(\eta)=2\tan^{-1}\alpha\eta-2\tan^{-1}\eta , \tag{A5}$$

where $\eta=y/s$, and α is a constant to be found. Then

$$\sin\varphi=-\frac{2\eta(1-\alpha)}{1+\alpha}\left[\frac{1}{1+\eta^2}+\frac{\alpha}{1+\alpha^2\eta^2}\right] . \tag{A6}$$

Substituting Eqs. (A5) and (A6) into Eq. (17), and making use of the identity

$$\int_{-\infty}^{\infty}\frac{dx}{(1+x^2)(y-x)}=\frac{\pi y}{1+y^2} , \tag{A7}$$

we can reduce the integral equation (17) to the following algebraic form:

$$\frac{2\alpha^2\eta}{1+\alpha^2\eta^2}-\frac{2\eta}{1+\eta^2}+\frac{2\eta}{1+\eta^2}+\varepsilon\sin\varphi=0 , \tag{A8}$$

where $\varepsilon=s/l$, and $\sin\varphi$ is given by Eq. (A6). If one takes $\alpha=\epsilon$, the ansatz (A5) cancels the leading terms proportional to $\eta/(1+\eta^2)$ and $\eta\alpha^2/(1+\alpha^2\eta^2)$ in Eq. (A8), while small terms of higher order in ε remain [although the first term in Eq. (A8) is formally proportional to ϵ^2, the small parameter ε cancels at $\eta\gg1/\varepsilon$, and all the leading terms decrease as $1/\eta$]. Therefore, Eq. (A5) is an asymptotically exact solution of Eq. (17) at $\varepsilon\to0$, so at $\varepsilon\ll1$ the function $\varphi(y)$ can be expanded in a power series of ϵ. The next iteration can be written in the form $\varphi=\varphi_0+\varphi_1$, where φ_0 is given by Eq. (A5), and φ_1 is a small correction of order ε which comes from the terms $\epsilon\eta/(1+\eta^2)$ and $\eta\epsilon^3/(1+\alpha^2\eta^2)$ in Eq. (A8). To calculate φ_1, we linearize Eq. (17) in φ_1 and obtain the following equation, written with the linear accuracy in ε:

$$\int_{-\infty}^{\infty}\frac{\varphi_1'(\xi)d\xi}{\eta-\xi}=2\pi\varepsilon\left[\frac{\eta}{1+\eta^2}-\frac{\alpha^2\eta}{1+\alpha^2\eta^2}\right] , \tag{A9}$$

$$\alpha=\varepsilon-\varepsilon^2 . \tag{A10}$$

According to Eq. (A7), Eq. (A9) has the solution $\varphi_1=2\varepsilon(\tan^{-1}\eta-\tan^{-1}\alpha\eta)$, therefore

$$\varphi=2(1-\varepsilon)(\tan^{-1}\alpha\eta-\tan^{-1}\eta) . \tag{A11}$$

In terms of the vortex-antivortex analogy shown in Fig. 1, the factor $(1-\epsilon)$ in Eq. (A11) results in the smaller magnetic flux $\phi=(1-\epsilon)\phi_0$ of image vortices as compared to ϕ_0 [see Eq. (8)].

The above iteration scheme enables one to calculate the higher-order corrections $\varphi(y)=\varphi(y)+\varphi_1(y)+\varphi_2(y)+\cdots$, where $\varphi_n(y)\propto\epsilon^n\ll1$. This procedure, however, is quite cumbersome, so we propose here a simple interpolation formula for $\varphi(y)$ which gives the correct asymptotics of the solution of the nonlinear Eq. (10) in two limiting cases $s\ll l$ and $s\gg l$, respectively. This can be done if one takes $\alpha=\varepsilon/(1+\varepsilon)$, or

$$\alpha=\frac{s}{l+s} . \tag{A12}$$

In this case Eq. (A5) not only is a solution of Eq. (17) at $s\ll l$, but also reduces to another exact asymptotics (16) at $s\gg l$, after expanding $\tan^{-1}[\eta\varepsilon/(1+\varepsilon)]$ in a power series in $1/\varepsilon$. This approach also reproduces Eq. (A10) at $\varepsilon\ll1$, but does not account for the small difference between ϕ and ϕ_0 which does not affect the qualitative interpretation of $f_\perp$ given in the text, since the total magnetic flux ϕ remains equal to ϕ_0.

APPENDIX B: CALCULATION OF $F(s)$

We calculate F_m by substituting Eqs. (18)–(20) into Eq. (13), in which the integral term can be transformed by means of the identity:

$$\int_0^{\infty}\frac{\ln(a+bx^2)}{c+dx^2}dx=\frac{\pi}{\sqrt{cd}}\ln\left[a^{1/2}+\left[\frac{bc}{d}\right]^{1/2}\right] . \tag{B1}$$

Then we obtain after some algebra

$$F_m=\left[\frac{\phi_0}{4\pi\lambda}\right]^2\left[\ln\frac{\lambda s}{(s+l)\xi}+\gamma_A\right] , \tag{B2}$$

where the constant $\gamma_A=0.497$ is chosen in such a way that at $s\gg l$, Eq. (B2) would give the line energy of the A fluxon with the account of the core energy.[27]

To calculate the Josephson energy F_J, we first calculate the quantity $1-\cos\varphi$, where $\varphi(y)$ is given by Eq. (18). This yields

$$1-\cos\varphi=\frac{2l}{l+2s}\left[\frac{(l+s)^2}{(l+s)^2+y^2}-\frac{s^2}{s^2+y^2}\right] . \tag{B3}$$

Substituting Eq. (B3) into Eq. (11), one obtains

$$F_J=\left[\frac{\phi_0}{4\pi\lambda}\right]^2\frac{l}{2s+l} . \tag{B4}$$

By adding Eqs. (B3) and (B4), we arrive at Eq. (21).

*Present address: National Institute of Standards and Technology, Electromagnetic Technology Division, Boulder, Colorado 80303.

[1]P. J. Lee and D. C. Larbalestier, J. Mater. Sci. **23**, 3951 (1988); C. Meingast and D. C. Larbalestier, J. Appl. Phys. **66**, 5971 (1989); L. D. Cooley, P. D. Jablonski, P. J. Lee, and D. C. Larbalestier, Appl. Phys. Lett. **56**, 2248 (1991).

[2]M. Suenaga, in *Superconductor Materials Science,* edited by S. Foner and B. B. Schwartz (Plenum, New York, 1981), p. 201.

[3]C. Rossel and O. Fisher, J. Phys. F **14**, 455 (1984).

[4]L. A. Bonney, T. C. Willis, and D. C. Larbalestier, IEEE Appl. Supercond. **3**, 1583 (1993).

[5]K. E. Gray, R. T. Kampwirth, D. W. Capone II, and R. Vaglio, Physica B **135**, 164 (1985); K. E. Gray, R. T. Kampwirth, J. M. Murduck, and D. W. Capone II, Physica C **152**, 445 (1988).

[6]B. M. Lairson, S. K. Streiffer, and J. C. Bravman, Phys. Rev. B **42**, 10 067 (1990).

[7]S. Fleshler, W-K. Kwok, U. Welp, V.M. Vinokur, M. K. Smith, J. Downey, and G. W. Crabtree, Phys. Rev. B **47**, 14 448 (1993).

[8]J. N. Li, A. A. Menovsky, and J. J. M. Franse, Phys. Rev. B **48**, 6612 (1993).

[9]Y. Matsui, H. Maeda, Y. Tanaka, and S. Horiuchi, Jpn. J. Appl. Phys. **27**, L361 (1988); Y. Bando, T. Kijima, T. Kitami, J. Tanaka, F. Izumi, and M. Yokoyama, *ibid.* **27**, 358 (1988).

[10]Y. Feng, K. E. Hautanen, Y. E. High, D. C. Larbalestier, R. Ray II, E. E. Hellstrom, and S. E. Babcock, Physica C **192**, 293 (1992).

[11]A. Umezawa, Y. Feng, H. S. Edelman, Y. E. High, D. C. Larbalestier, Y. S. Sung, E. E. Hellstrom, and S. Fleshler, Physica C **198**, 261 (1992); A. Umezawa, Y. Feng, H. S. Edelman, T. C. Willis, J. A. Parrell, and D. C. Larbalestier, *ibid.* **219**, 378 (1994).

[12]B. Hensel, J.-C. Grivel, A. Jeremie, A. Perin, A. Pollini, and R. Flukiger, Physica C **205**, 329 (1993).

[13]L. N. Bulaevskii, J. R. Clem, L. I. Glazman, and A. P. Malozemoff, Phys. Rev. B **45**, 2545 (1992); L. N. Bulaevskii, L. L. Daemen, M. P. Maley, and J. Y. Coutler, *ibid.* **48**, 13 798 (1993).

[14]M. Daeumling, J. M. Seuntjens, and D. C. Larbalestier, Nature (London) **346**, 332 (1990).

[15]M. Tinkham and C. J. Lobb, in *Solid State Physics: Advances in Research and Applications,* edited by H. Ehrenreich and D. Turnbull (Academic, New York, 1989), Vol. 42, p. 91.

[16]A. Barone and G. Paterno, *Physics and Applications of the Josephson Effect* (Wiley, New York, 1982).

[17]A. Gurevich, Phys. Rev. B **46**, 3187 (1992); *ibid.* **48**, 12 857 (1993).

[18]J. R. Clem and M. W. Coffey, Phys. Rev. B **42**, 6209 (1990); M. W. Coffey and J. R. Clem, *ibid.* **44**, 6903 (1991); J. R. Clem, M. W. Coffey, and Z. Hao, *ibid.* **44**, 2732 (1991).

[19]R. G. Mints and I. B. Snapiro, Phys. Rev. B **49**, 6188 (1994).

[20]D. Stauffer, Phys. Rep. **54**, 2 (1979); *Introduction to the Percolation Theory* (Taylor and Frances, London, 1985).

[21]Yu. M. Aliev, V. P. Silin, and S. A. Uryupin, Sverkhprovodimost' (KIAE) **5**, 228 (1992) [Superconductivity **5**, 228 (1992)]; Yu. M. Aliev and V. P. Silin, Zh. Eksp. Teor. Fiz. **104**, 2526 (1993) [Sov. Phys. JETP **77**, 142 (1993)].

[22]E. H. Brandt, Phys. Rev. Lett. **57**, 1347 (1986).

[23]P. H. Kes, A. Pruymboom, J. van den Berg, and J. A. Mydosh, Cryogenics **29**, 228 (1989).

[24]A. A. Golubov and A. V. Ustinov, Phys. Lett. A **162**, 409 (1992).

[25]A. A. Abrikosov, *Fundamentals of the Theory of Metals* (North-Holland, Amsterdam, 1988).

[26]I. S. Gradshteyn and I. M. Ryzhik, *Tables of Integrals, Series and Products* (Academic, New York, 1980).

[27]C.-R. Hu, Phys. Rev. B **6**, 1756 (1972).

[28]As follows from the more accurate Eq. (A11), the "image" vortex and antivortex have the effective flux $\phi_e = \pm(1 - s/l)\phi_0$ which is slightly *smaller* than ϕ_0. This does not affect the qualitative analysis given in the text for $s \ll l$, since the difference between ϕ_e and ϕ_0 is small, and the total magnetic flux ϕ remains equal to ϕ_0.

[29]C. P. Bean and J. D. Livingston, Phys. Rev. Lett. **12**, 14 (1964).

[30]A. M. Campbell and J. E. Evetts, Adv. Phys. **21**, 199 (1972).

[31]R. Fehrenbacher, V. B. Geshkenbein, and G. Blatter, Phys. Rev. B **45**, 5450 (1992).

[32]P. Pincus, A. C. Gossard, A. C. Jaccarino, and J. H. Wernick, Phys. Lett. **13**, 21 (1964); V. V. Schmidt, Zh. Eksp. Teor. Fiz. **46**, 649 (1964) [Sov. Phys. JETP **19**, 440 (1964)].

[33]E. L. Kramer, J. Appl. Phys. **44**, 1360 (1976).

[34]L. B. Ioffe and A. I. Larkin, Zh. Eksp. Teor. Fiz. **81**, 707 (1981) [Sov. Phys. JETP **54**, 378 (1981)].

[35]A. Pruymboom, P. H. Kes, E. van der Drift, and S. Radelaar, Phys. Rev. Lett. **52**, 662 (1988).

[36]A. Gurevich, Phys. Rev. B **42**, 4857 (1990); A. Gurevich, H. Kupfer, and C. Keller, Europhys. Lett. **15**, 789 (1991); Supercond. Sci. Technol. **4**, S91 (1991).

[37]R. Wordenweber, Phys. Rev. B **46**, 3076 (1992).

[38]H. J. Jensen, Y. Brecht, and A. Brass, J. Low Temp. Phys. **74**, 293 (1989); H. J. Jensen, A. Brass, A.-C. Shi, and A. J. Berlinsky, Phys. Rev. B **41**, 6394 (1990); Y. Brecht, B. Doucot, H. J. Jensen, and A. C. Shi, *ibid.* **42**, 2116 (1990).

[39]D. Dominguez, Phys. Rev. Lett. **72**, 3096 (1994).

[40]G. Blatter, J. Rhyner, and V. M. Vinokur, Phys. Rev. B **43**, 7826 (1991).

[41]E. B. Sonin, Phys. Rev. B **48**, 7826 (1993).

[42]N. Uchida, K. Empuku, Y. Matsugaki, S. Tomita, F. Irie, and K. Yoshida, J. Appl. Phys. **54**, 5287 (1983); N. Uchida, K. Enpuku, K. Yoshida, and F. Irie, *ibid.* **56**, 2558 (1984).

[43]S. L. Miller, K. R. Biagi, J. R. Clem, and D. K. Finnemore, Phys. Rev. B **31**, 2684 (1985).

[44]M. V. Fistul', Pis'ma Zh. Eksp. Teor. Fiz. **52**, 823 (1990) [Sov. Phys. JETP Lett. **52**, 192 (1990)]; V. N. Gubankov, M. P. Lisitskii, I. L. Serpuchenko, and M. V. Fistul', Zh. Eksp. Teor. Fiz. **100**, 1326 (1991) [Sov. Phys. JETP **73**, 734 (1991)].

[45]P. G. de Gennes, Rev. Mod. Phys. **36**, 225 (1964).

[46]C. A. Duran, P. L. Gammel, R. Wolfe, V. J. Fratello, D. J. Bishop, J. R. Rice, and D. M. Ginsberg, Nature (London) **357**, 474 (1992).

[47]M. Turchinskaya, D. L. Kaiser, F. W. Gayle, A. J. Shapiro, A. Roytburd, V. Vlasko-Vlasov, A. Polyanskii, and V. Nikitenko, Physica C **216**, 205 (1993).

[48]L. A. Dorosinskii, V. I. Nikitenko, A. A. Polyanskii, and V. K. Vlasko-Vlasov, Physica C **219**, 81 (1994).

[49]J. D. Livingston, Appl. Phys. Lett. **8**, 319 (1966).

[50]C. Baker and J. Sutton, Philos. Mag. **19**, 1223 (1968).

[51]H. Kupfer, I. Apfelstedt, R. Flukiger, C. Keller, R. Meier-Hirmer, B. Runtsch, A. Turowski, U. Wiech, and T. Wolf, Cryogenics **29**, 268 (1989); C. Keller, H. Kupfer, R. Meier-Hirmer, U. Wiech, V. Selvamanickam, and K. Salama, *ibid.* **30**, 401 (1990).

[52]J. L. Vargas and D. C. Larbalestier, Appl. Phys. Lett. **60**, 1741 (1992).

[53]M. S. Osofsky, J. L. Cohn, E. F. Skelton, M. M. Miller, R. J. Soulen, Jr., S. A. Wolf, and T. A. Vanderah, Phys. Rev. B **45**, 4916 (1992).

[54]J. G. Ossandon, J. R. Thompson, D. K. Christen, B. C. Sales, H. R. Kerchner, J. O. Thomson, Y. R. Sun, K. W. Lay, and J. E. Tkaczyk, Phys. Rev. B **45**, 12 534 (1992).

[55]L. Klein, E. R. Yakoby, Y. Yeshurun, A. Erb, G. Muller-Vogt, V. Breit, and H. Wuhl, Phys. Rev. B **49**, 4403 (1994).

[56]N. Chukumoto, M. Konzcykowski, N. Motohira, and A. P. Malozemoff, Phys. Rev. Lett. **69**, 1260 (1992).

[57]L. Krusin-Elbaum, L. Civale, V. M. Vinokur, and F. Holtzberg, Phys. Rev. Lett. **69**, 2280 (1992).

[58]Y. Yeshurun, N. Bontemps, L. Burlachkov, and A. Kapitulnik, Phys. Rev. B **49**, 1548 (1994).

[59]A. E. Koshelev and P. H. Kes, Phys. Rev. B **48**, 6539 (1993).

[60]L. D. Cooley, Ph.D. thesis, University of Wisconsin-Madison, 1993.

[61]J. S. Satchell *et al.*, Nature (London) **334**, 331 (1988); T. Nishizaki *et al.*, Physica C **181**, 223 (1991).

[62]A. Gurevich, A. E. Pashitski, H. S. Edelman, and D. C. Larbalestier, Appl. Phys. Lett. **62**, 1688 (1993).

[63]H. Yamasaki, K. Endo, S. Kosaka, M. Umeda, S. Yoshida, and K. Kajimura, Phys. Rev. Lett. **70**, 3331 (1993).

[64]A. Umezawa, W. Zhang, A. Gurevich, Y. Feng, E. E. Hellstrom, and D. C. Larbalestier, Nature (London) **364**, 129 (1993).

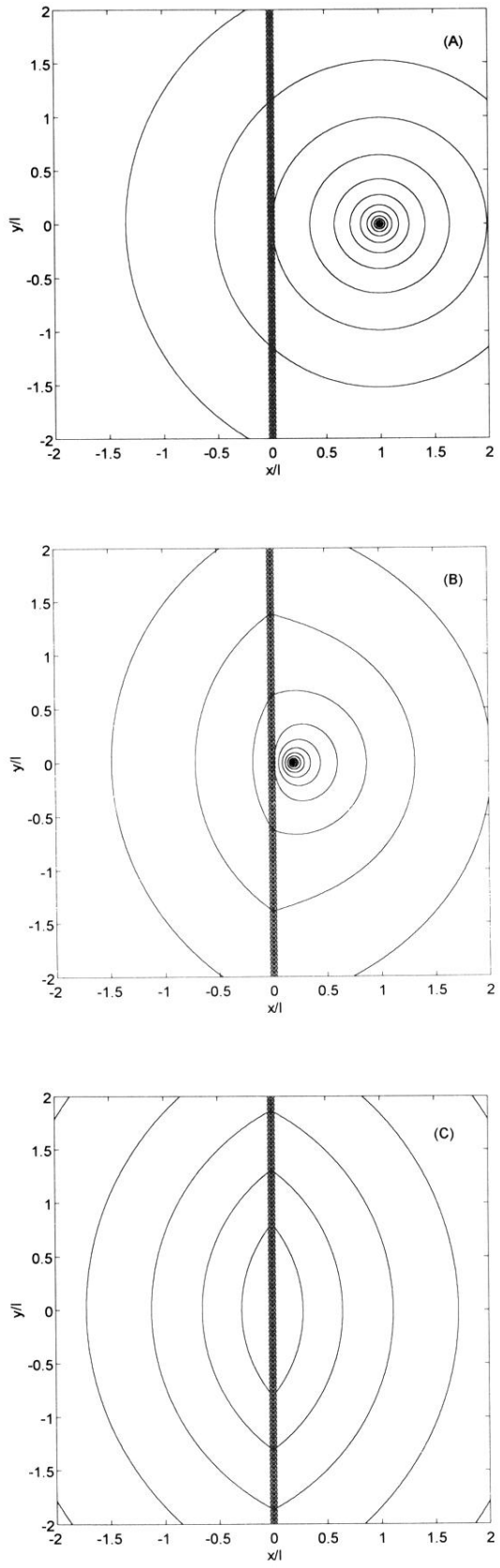

FIG. 2. Successive changes of the current distribution around the A vortex as it moves toward the planar defect. Shown are the current lines described by Eqs. (19) and (20) at $s=l$ (a), $s=0.2l$ (b), and $s=0$ (c).